Lanthanide (Eu^{3+}, Tb^{3+}) functionalized SBA-15 through modified hexafluoroacetylacetone linkage: Covalently bonding construction, physical characterization, and luminescent properties

Ya-Juan Li,[a] Xudong Yu, Xiaojing Wang, and Minli Yang
College of Science, Hebei University of Science and Technology, Shijiazhuang 050080, People's Republic of China

(Received 9 October 2013; accepted 27 January 2014)

New organic/inorganic mesoporous luminescent hybrid materials containing lanthanide (Eu, Tb) complexes chemically bonded to mesoporous SBA-15 [a kind of mesoporous silica with two-dimensional hexagonal (*P6mm*) structure] have been successfully synthesized by co-condensation of the modified hexafluoroacetylacetone (HFAASi) and tetraethoxysilane (TEOS) in the presence of Pluronic P123 surfactant as a template. The luminescent properties of these resulting mesoporous hybrid materials [denoted as Ln(HFAASi-SBA-15)$_3$phen, Ln = Eu, Tb; phen = 1,10-phenanthroline] were characterized by Fourier transform infrared, small-angle powder x-ray diffraction, N_2 adsorption measurements, transmission electron microscope, ultraviolet-visible diffuse reflection absorption spectra, and photoluminescent spectra, and the results exhibit that they all have uniformity in mesostructure and high surface area. Moreover, the mesoporous hybrid materials Eu(HFAASi-SBA-15)$_3$phen and Tb(HFAASi-SBA-15)$_3$phen exhibit the characteristic luminescence of Eu^{3+} and Tb^{3+}, respectively, indicating that the effective intramolecular energy transfer between HFAASi and the lanthanide ions has been achieved.

I. INTRODUCTION

Lanthanide complexes with organic ligands have long been the subject of extensive research for their special luminescence properties with high color purity and long lifetimes as well as high quantum efficiency, which can be expected to have potential applications in a variety of fields such as luminescent sensors, lasers, optical amplification, organic-light emitting diodes, and light-conversion molecular devices.[1–4] However, due to their poor thermal stabilities and low mechanical strength, the lanthanide complexes have been excluded from practical applications. One solution is to incorporate the lanthanide complexes into stable host matrices such as inorganic gel or organic polymer to construct organic–inorganic hybrid materials, which not only improved the photo and thermal stabilities of the complexes but also avoided the self-quenching resulting from the concentration effect.[5–7] The mesoporous molecular sieves used as a support for rare earth complexes have attracted considerate attention because they possess properties such as photostability, rigidity, and well-defined hydrophilic/hydrophobic properties, which allow for sophisticated tuning of the rare earth complex microenvironment.[8] Among them, SBA-15 has certainly become one of the most attractive hosts due to its large pore size, thick walls, adjustable pore size from 3 to 30 nm, high hydrothermal and thermal stability.[9,10] Until recently, Zhang[11–13] and Yan[14–18] group reported the synthesis and luminescent properties of lanthanide complexes chemically bonded to mesoporous silica SBA-15. It is shown that excellent visible-luminescent properties can be obtained via linking the lanthanide complexes to mesoporous silica materials.

In this paper, hexafluoroacetylacetone (HFAA)-functionalized SBA-15 mesoporous hybrid (HFAASi-SBA-15) was prepared, in which HFAA was covalently bonded to the framework SBA-15 by co-condensation of modified HFAA (denoted as HFAASi) and tetraethoxysilane (TEOS) in the presence of Pluronic P123 surfactant as a template. The highly luminescent ternary lanthanide (Eu^{3+}, Tb^{3+}) complex on functionalized SBA-15, denoted as Ln(HFAASi-SBA-15)$_3$phen (Ln = Eu, Tb), was obtained by introducing Ln^{3+} and 1,10-phenanthroline (phen) into the hybrid material HFAASi-SBA-15 through chemically bond assembling method. Full characterization and detail studies of luminescent properties of all these synthesized hybrid materials were investigated.

II. EXPERIMENTAL SECTION

A. Chemicals

Europium and terbium nitrates were obtained by dissolving their respective oxides (Eu_2O_3 and Tb_4O_7) in concentrated nitric acid. Hexafluoroacetylacetone (HFAA),

[a]Address all correspondence to this author.
e-mail: liyajuan0820@163.com
DOI: 10.1557/jmr.2014.33

 © Materials Research Society 2014

https://doi.org/10.1557/jmr.2014.33 Published online by Cambridge University Press

3-(triethoxysilyl)-propyl isocyanate (TESPIC), and Pluronic P123 ($EO_{20}PO_{70}EO_{20}$) were purchased from the Lancaster company (Shanghai, China). Tetraethoxysilane (TEOS, Aldrich, Shanghai, China) was distilled and stored under nitrogen atmosphere. The solvent tetrahydrofuran (THF) was introduced after desiccation with anhydrous calcium chloride. All the other reagents are analytically pure.

B. Synthesis

1. Synthesis of HFAA-functionalized SBA-15 mesoporous material (HFAASi-SBA-15)

The modified precursor HFAASi was synthesized according to the procedure reported in the literature,[19] described as follows: first, HFAA (1 mmol, 0.21 g) was dissolved in 20 mL of dehydrate THF with stirring, and NaH (2 mmol, 0.048 g) was added to the solution. Two hours later, 2.0 mmol (0.49 g) of TESPIC was then added to the above mixture solution by drops for half an hour. The whole mixture was refluxing at 70°C under an atmosphere of argon for 12 h. A yellow oil liquid sample, i.e., the precursor HFAASi was obtained after isolation and purification. The mesoporous material HFAASi-SBA-15 was prepared from acidic mixture with the following molar composition: 0.0172 P123: 0.96 TEOS: 0.04 HFAASi: 6 HCl: 208.33 H_2O. 1.0 g of P123 was dissolved in 7.5 g of deionized water and 30 g of 2 M HCl solution at 35 °C under vigorous stirring. A mixture of TEOS and HFAASi was added to the above solution, which was stirred at 35 °C for 24 h and transferred into a Teflon bottle sealed in an autoclave, which was then heated at 100 °C for 48 h. The solid product was filtrated, washed thoroughly with deionized water, and air-dried at 60 °C for 10 h. Removal of copolymer surfactant P123 was conducted through Soxhlet extraction with ethanol under reflux for 48 h to give the sample denoted as HFAASi-SBA-15.

2. Synthesis of SBA-15 mesoporous material chemically bonded with the ternary Ln^{3+} complexes [denoted as Ln(HFAASi-SBA-15)$_3$phen (Ln = Eu, Tb)]

The sol–gel-derived hybrid mesoporous material Ln(HFAASi-SBA-15)$_3$phen was prepared as follows: while being stirred, HFAASi-SBA-15 was soaked in an appropriate amount of $Ln(NO_3)_3$ and 1,10-phenanthroline (phen) ethanol solution with the molar ratio of Ln^{3+}:HFAASi-SBA-15:phen = 1:3:1. The mixture was stirred at room temperature for about 12 h followed by filtration and extensive washing with EtOH. The resulting materials Ln(HFAASi-SBA-15)$_3$phen were dried at 60 °C under vacuum overnight. The predicted structure of Ln(HFAASi-SBA-15)$_3$phen was obtained as outlined in Fig. 1.

C. Characterization

Fourier transform infrared (FTIR) spectra were measured within the 4000–400 cm^{-1} region on a Nicolet 6700 spectrophotometer (Thermo Electron Corporation, MA) with the KBr pellet technique. Nitrogen (N_2) adsorption/desorption isotherms were measured by using a Nova 2000 analyzer (Quantachrome, Beijing, China) at the liquid nitrogen temperature. Before the measurements, the sample was outgassed for 3 h at 423 K. Surface areas were calculated by the Brunauer–Emmett–Teller (BET) method and pore size distributions were evaluated from the desorption branches of the nitrogen isotherms using the Barrett–Joyner–Halenda (BJH) model. X-ray powder diffraction patterns were recorded on a Rigaku D/max2500VB+/PC diffractometer (Hitachi Limited, Tokyo, Japan) equipped with a Cu anode in a 2θ range from 0.6° to 6°. Transmission electron microscope (TEM) observation was made on a JEOL2011 microscope (Hitachi Limited, Tokyo, Japan) operated at 200 kV and on a JEM-4000EX microscope (Hitachi Limited, Tokyo, Japan) operated at 400 kV. Reflectivity spectra were recorded on a UV-2501 spectrometer (Shimadzu, Tokyo, Japan) equipped with a diffuse reflectance accessory. The fluorescence excitation and emission spectra were obtained on a Hitachi F-4500 spectrophotometer (Hitachi Limited, Tokyo, Japan). The luminescence lifetime measurements were measured with an Edinburgh FLS920 phosphorimeter (Edinburgh Instruments Ltd., UK) using a 450 W xenon lamp as the excitation source.

III. RESULTS AND DISCUSSION

A. FTIR spectra

The presence of the organic ligand HFAA covalently bonded to the mesoporous SBA-15 was characterized by FTIR spectra. The FTIR spectra for HFAA (a), the precursor HFAASi (b), and HFAA-functionalized mesoporous hybrid material HFAASi-SBA-15 (c) are shown in Fig. 2. From a to b, it can be observed that the stretching of $–CH_2–$ at 3257 cm^{-1} (a) was replaced by the peaks at 2981, 2930, and 2887 cm^{-1} (b), which originated from three methylene groups of TESPIC. In addition, the spectrum of HFAASi is dominated by ν (C–Si, 1193 cm^{-1}) and ν (Si–O, 1081 cm^{-1}) absorption bands, characteristic of trialkoxylsilyl functions, which suggests formation of the siloxane bonds. The band centered at 3430 cm^{-1} corresponds to the stretching vibration of grafted –NH– groups. Besides, the bending vibration (δ_{NH}, 1537 cm^{-1}) further proves the formation of amide groups. New bands at 1770 and 1679 cm^{-1} in curve b were due to the absorptions of the C=O of TESPIC, proving that TESPIC was successfully grafted onto the ligand HFAA. In Fig. 2(c), the formation of Si–O–Si framework is evidenced by the broad bands located at 1081 cm^{-1} (ν_{as}, Si–O), 804 cm^{-1}

https://doi.org/10.1557/jmr.2014.33 Published online by Cambridge University Press

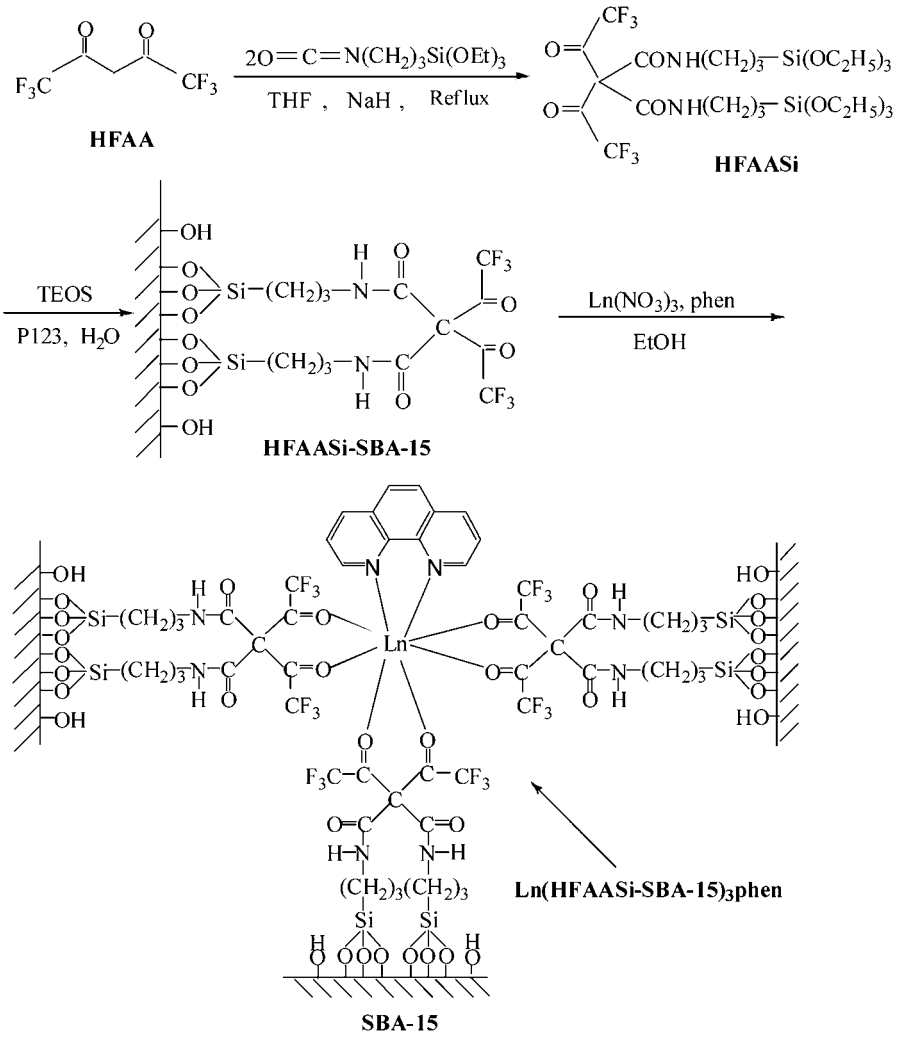


FIG. 1. Synthesis process and predicted structure of the ternary mesoporous hybrid material Ln(HFAASi-SBA-15)$_3$phen (Ln = Eu, Tb).

(ν_s, Si–O), and 462 cm^{-1} (δ, Si–O–Si), which is ascribed to the success of hydrolysis and copolycondensation (where ν represents stretching; δ, plane bending; s, symmetric; and as, asymmetric vibrations). Moreover, the bands at 1636 and 1493 cm^{-1} originating from –CONH– group of HFAASi, can also be observed in mesoporous hybrid material HFAASi-SBA-15 (c), which is consistent with the fact that the HFAA group in the framework remains intact after both the hydrolysis–condensation reaction and the surfactant extraction procedure.[11]

Figure 3 gives the FTIR spectra of SBA-15 (a), HFAASi-SBA-15 (b), Eu(HFAASi-SBA-15)$_3$phen (c), and Tb(HFAASi-SBA-15)$_3$phen (d). In the spectrum of the SBA-15 host material (a), the obvious absorption bands from –OH– (3446 cm^{-1}), Si–O–Si (ν_{as}, 1081 cm^{-1}; ν_s, 804 cm^{-1}), Si–OH (ν_s, 960 cm^{-1}), Si–O (δ, 462 cm^{-1}), and H_2O (1635 cm^{-1}) are present.[20,21] Compared with SBA-15, the mesoporous hybrid materials

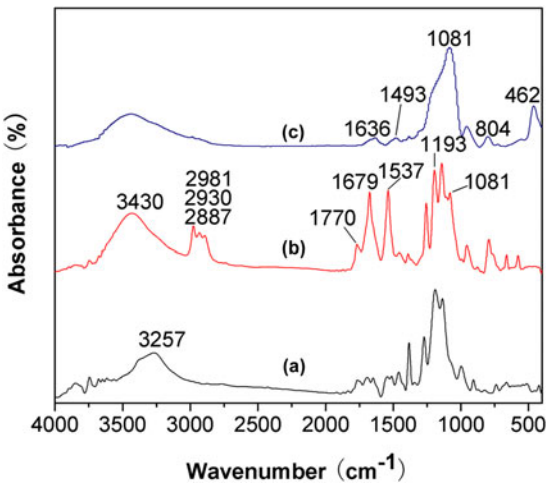


FIG. 2. FTIR spectra of HFAA (a), HFAASi (b), and HFAA-functionalized mesoporous hybrid HFAASi-SBA-15 (c).

https://doi.org/10.1557/jmr.2014.33 Published online by Cambridge University Press

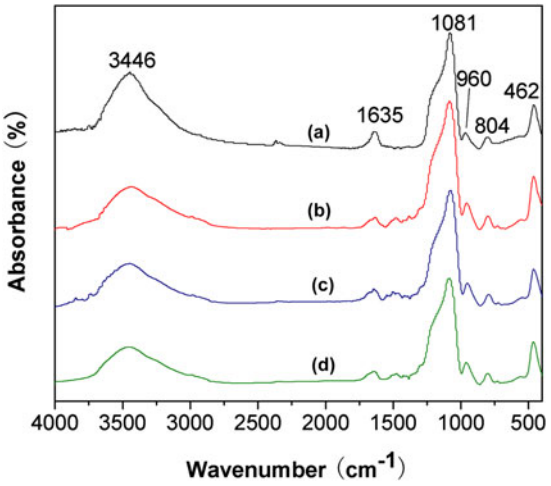


FIG. 3. FTIR spectra of SBA-15 (a), HFAASi-SBA-15 (b), Eu(HFAASi-SBA-15)$_3$phen (c), and Tb(HFAASi-SBA-15)$_3$phen (d).

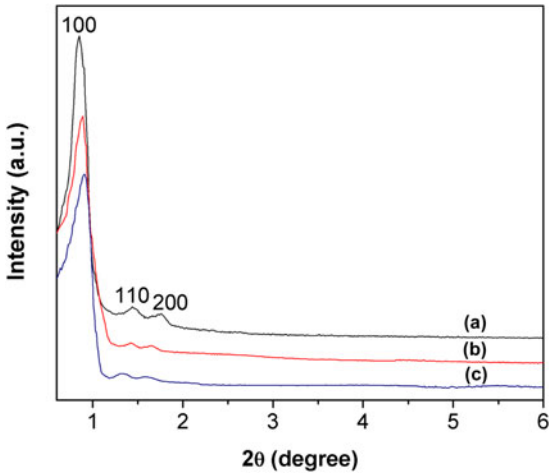


FIG. 4. SAXRD patterns of HFAASi-SBA-15 (a), Eu(HFAASi-SBA-15)$_3$phen (b) and Tb(HFAASi-SBA-15)$_3$phen (c).

HFAASi-SBA-15 and Ln(HFAASi-SBA-15)$_3$phen (Ln = Eu, Tb) not only show the similar absorption bands as the silica framework, but also the bands at the range of 2850–3000 cm^{-1} attributed to the vibrations of methylene –$(CH_2)_3$– and the bands at 1380–1630 cm^{-1} range originating from the –CONH– group of HFAASi, indicates that HFAASi has been grafted onto the wall of SBA-15.

B. X-ray diffraction

The small-angle powder x-ray diffraction (SAXRD) measurement is a very popular and efficient method to characterize the nanostructured host-guest hybrid materials. Figure 4 shows the SAXRD patterns of HFAASi-SBA-15 (a), Eu(HFAASi-SBA-15)$_3$ (b), and Tb(HFAASi-SBA-15)$_3$phen (c). These patterns exhibit three well-resolved diffraction peaks in the 2θ range of 0.6–2°, which can be indexed as (100), (110), and (200) reflections of a two-dimensional hexagonal structure (*p6mm*) of SBA-15 material. Compared with the SAXRD pattern of HFAASi-SBA-15 material, the d_{100} spacing values of Eu(HFAASi-SBA-15)$_3$phen and Tb(HFAASi-SBA-15)$_3$phen are nearly unchanged (see Table I), suggesting that their framework ordering has been retained well after the introduction of Ln^{3+}. However, it is worth noting that Ln^{3+} complex functionalized materials Eu(HFAASi-SBA-15)$_3$phen and Tb(HFAASi-SBA-15)$_3$phen appear slight decrease in diffraction intensity as compared with the parent HFAASi-SBA-15 material, which is probably because of the steric constraints introduced by the linking of ligands via complexation with the lanthanide ions, resulting in a larger heterogeneity of the pores.[22]

C. Nitrogen sorption measurement

The measurements of nitrogen adsorption/desorption isotherms further provide proof for the preservation of the ordered mesoporous structure upon the introduction of the lanthanide ion. The nitrogen adsorption/desorption isotherms of HFAASi-SBA-15 (a), Eu(HFAASi-SBA-15)$_3$phen (b), and Eu(HFAASi-SBA-15)$_3$phen (c) are presented in Fig. 5. All these samples exhibit type IV isotherm curves with a clear H1 type hysteresis at high relative pressure, characteristic of highly ordered mesoporous materials according to the IUPAC classification.[23–25] By using BET and BJH methods, the specific area and the pore size have been calculated. And the structural data of all these mesoporous hybrid materials (BET surface area, total pore volume, BJH average pore size, etc.) are summarized in Table I. It was observed that HFAASi-SBA-15 exhibits a smaller specific area, and a slightly smaller pore size and pore volume compared with those typically reported for pure SBA-15 mesoporous silica,[11] which might be due to the presence of both organic ligand HFAA on the pore surface and the cosurfactant effect of HFAASi, which interacts with surfactant and reduces diameter of the micelles.[26] Furthermore, upon introduction of Ln^{3+} into the HFAASi-SBA-15, the specific area, pore size, and pore volume of the hybrid materials containing Ln^{3+}

TABLE I. Textural data of SBA-15, HFAASi-SBA-15, Eu(HFAASi-SBA-15)$_3$phen and Tb(HFAASi-SBA-15)$_3$phen.[a]

Sample	d_{100} (nm)	a_0 (nm)	S_{BET} (m^2/g)	V (cm^3/g)	D (nm)	t (nm)
SBA-15	10.76	12.42	1197	1.81	7.39	5.03
HFAASi-SBA-15	10.38	11.99	638	0.84	5.84	6.15
Eu(HFAASi-SBA-15)$_3$phen	10.03	11.58	589	0.79	4.54	7.04
Tb(HFAASi-SBA-15)$_3$phen	9.81	11.33	564	0.76	4.53	6.80

[a]d_{100} is the d(100) spacing, a_0—the cell parameter ($a_0 = 2\ d_{100}/\sqrt{3}$), S_{BET}—the BET surface area, V—the total pore volume, D—the average pore diameter, and t—the wall thickness, calculated by $a_0 - D$.

https://doi.org/10.1557/jmr.2014.33 Published online by Cambridge University Press

were less than those of HFAASi-SBA-15. This further confirmed the incorporation of the Ln^{3+} complexes in the channels of SBA-15.

D. Transmission electron microscope

The hexagonal mesostructures of Eu(HFAASi-SBA-15)$_3$phen are further confirmed by TEM images (see Fig. 6). As presented in Fig. 6, the Eu^{3+} complex-functionalized mesoporous material Eu(HFAASi-SBA-15)$_3$phen presents a *P6mm* symmetry and regular hexagonal structure, which suggests that the mesostructure of Eu(HFAASi-SBA-15)$_3$phen can be substantially conserved after the complexation process. In addition, the distance between the centers of the mesopores is estimated to be around 10 nm, which is in good agreement with the value determined from the corresponding SAXRD data (see Table I).

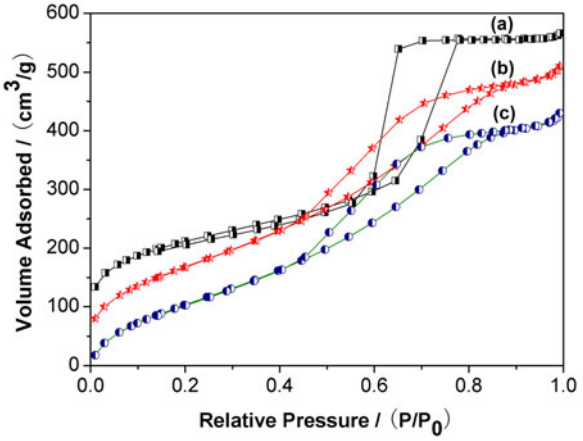


FIG. 5. N_2 adsorption–desorption isotherms of HFAASi-SBA-15 (a), Eu(HFAASi-SBA-15)$_3$phen (b) and Tb(HFAASi-SBA-15)$_3$phen (c).

E. Ultraviolet-visible diffuse reflection absorption spectra

The ultraviolet-visible diffuse reflectance spectroscopy of the lanthanide mesoporous hybrids is given in Fig. 7 [(a) for Eu(HFAASi-SBA-15)$_3$phen and (b) for Tb(HFAASi-SBA-15)$_3$phen]. It is observed that both the spectra exhibit a broad absorption band in the UV-vis range (200–500 nm), which corresponds to transition from the ground state of the organic ligand to the first excited state ($S_0 \rightarrow S_1$). Following Dexter's exchange energy transfer theory,[27] the luminescence intensity of hybrid materials depends on the matching degree between the triplet-state energy of ligand and excited-state energy of lanthanide ion. In terms of the above phenomena, it can be primarily predicted that the energy levels difference between HFAASi and lanthanide ions is suited and appropriate so that the organic ligand can absorb abundant energy in ultraviolet-visible extent to transfer the energy to the corresponding rare earth ions. Then the final hybrid materials can be expected to have excellent luminescence, which is proved by the emission spectra of these materials (see Figs. 8 and 9). In addition, the inverse peak at 614 nm for Eu(HFAASi-SBA-15)$_3$phen and 545 nm for Tb(HFAASi-SBA-15)$_3$phen, is the characteristic emission of europium and terbium ions, respectively.

F. Photoluminescence properties

The luminescence behavior of lanthanide mesoporous hybrid materials has been investigated at room temperature. The fluorescent excitation and emission spectra of europium mesoporous hybrid material are given in Fig. 8. The excitation spectrum of Eu(HFAASi-SBA-15)$_3$phen was obtained by monitoring the strongest emission wave length of Eu^{3+} ion at 614 nm. The excitation spectrum displays a large broad band ascribed to the excited states of

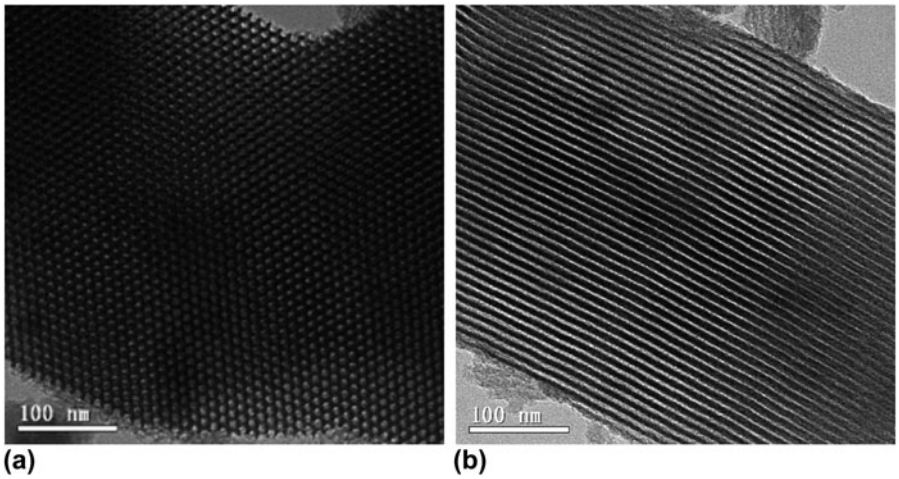


FIG. 6. HRTEM images of Eu(HFAASi-SBA-15)$_3$phen recorded along the [100] (a) and [110] (b) zone axes.

https://doi.org/10.1557/jmr.2014.33 Published online by Cambridge University Press

the ligands (220–370 nm, with one component at 351 nm) and a series of narrow lines attributed to transitions between the $^7F_0$ levels and the $^5L_6$, and $^5D_{1,2}$ excited states. The higher intensity of the broad-band excitation component with respect to that of the intra-$4f^6$ lines indicates that the Eu^{3+} sensitization process is more efficient than the direct intra-$4f^6$ excitation. So the emission spectrum was measured under excitation wave length of 351 nm. As a result, five sharp emission peaks at 579, 591, 614, 648, and 684 nm were seen, which are corresponding to the $^5D_0 \rightarrow {}^7F_J$ ($J = 0, 1, 2, 3, 4$) transitions of Eu^{3+}, respectively. Among these transitions, the $^5D_0 \rightarrow {}^7F_2$ transition at about 614 nm shows the most prominent emission. It is well known that the $^5D_0 \rightarrow {}^7F_2$ transition belongs to a typical electric dipole transition and strongly varies with the local symmetry of Eu^{3+}, whereas the $^5D_0 \rightarrow {}^7F_1$ transition corresponds to a parity-allowed magnetic dipole transition, which is independent of the host material. The intensity ratio of the red and orange is sensitive to the symmetry around Eu^{3+}. When the ratio is higher, europium ion occupies a lower symmetry microenvironment.[27–29] The intensity ratio of the two lines ($^5D_0 \rightarrow {}^7F_2/{}^5D_0 \rightarrow {}^7F_1$) is about 5.14, which indicates that the Eu^{3+} ion is not at the center of an asymmetric coordination field.

Figure 9 shows the excitation and emission spectra for terbium mesoporous hybrid Tb(HFAASi-SBA-15)$_3$phen. The excitation spectrum of the material was obtained by monitoring the emission of the Tb^{3+} ions at 545 nm, which exhibits broad excitation band centered at 349 nm in the ultraviolet region, corresponding to the ligand-to-metal resonant energy transfer caused by interaction between the organic groups and the rare-earth ions.[30–32] No apparent *f–f* transitions could be observed in the spectra. This indicates that an effective energy transfer occurs from the ligands to the central Tb^{3+} ions. Excitation at 349 nm provides the typical luminescence of Tb^{3+} ion at 490, 541, 583, and 621 nm, corresponding to $^5D_4 \rightarrow {}^7F_J$ transitions ($J = 6$, 5, 4, and 3, respectively). As a result, the strong green luminescence was observed in the emission spectra. The mesoporous hybrid materials show relatively strong emissions due to the chemically covalently bonded molecular Si–O network structure between the complexes and the mesoporous silica.

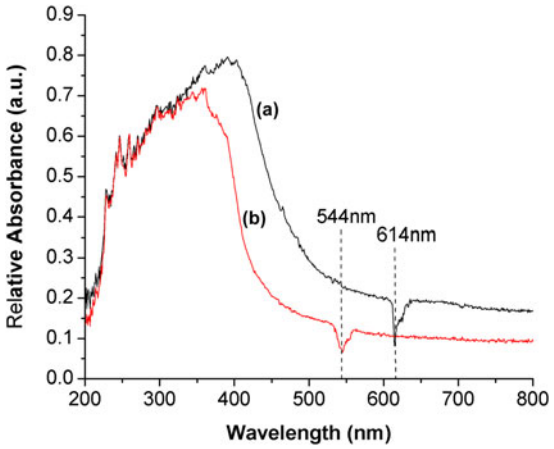


FIG. 7. The ultraviolet-visible diffuse reflection absorption spectra of Eu(HFAASi-SBA-15)$_3$phen (a) and Tb(HFAASi-SBA-15)$_3$phen (b).

G. Luminescence decay times (τ) and emission quantum efficiency (η)

To further discuss the photophysical properties of the resulting mesoporous materials, the typical decay curves of the europium and terbium mesoporous hybrid materials are measured, and they can be described as a single exponential ($\ln(S_{(t)}/S_0) = -k_1 t = -t/\tau$), indicating that Eu^{3+} and Tb^{3+} ions occupy the same average coordination environment. The resulting lifetime data of rare earth mesoporous hybrid materials are given in Table II. It was found that the mesoporous hybrid material Eu(HFAASi-SBA-15)$_3$phen presents longer luminescent lifetime than the hybrid material Tb(HFAASi-SBA-15)$_3$phen, suggesting that HFAASi is more suitable for the luminescence of Eu^{3+} than that of Tb^{3+}.

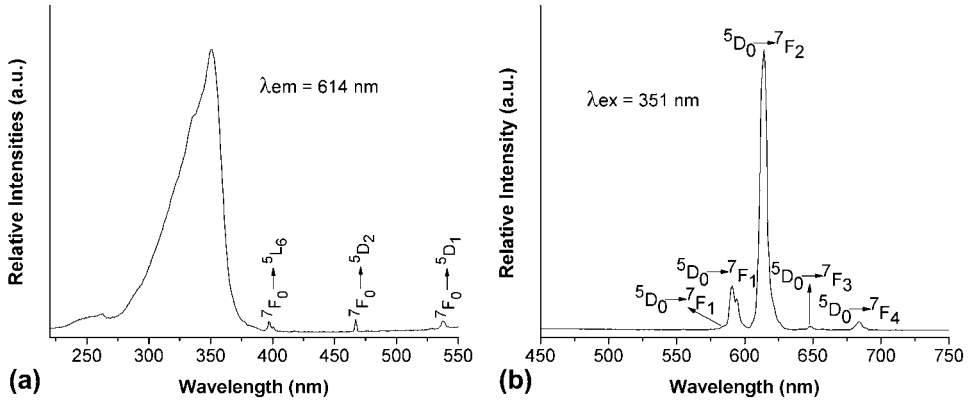


FIG. 8. The excitation spectra (a) and emission spectra (b) of Eu(HFAASi-SBA-15)$_3$phen.

https://doi.org/10.1557/jmr.2014.33 Published online by Cambridge University Press

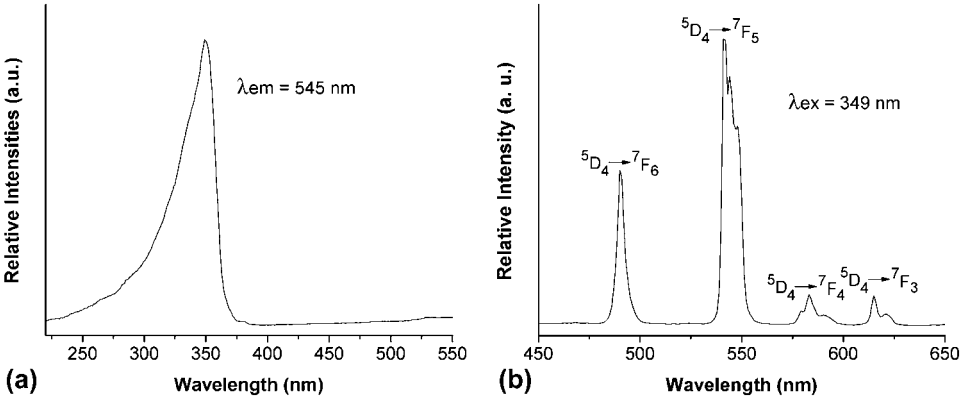


FIG. 9. The excitation spectra (a) and emission spectra (b) of Tb(HFAASi-SBA-15)$_3$phen.

TABLE II. Luminescence data of the mesoporous hybrid materials.

System	I_{02}/I_{01}	τ (μs)[a,b]	$1/\tau$ (s^{-1})	A_r (s^{-1})	A_{nr} (s^{-1})	η (%)
Eu(HFAASi-SBA-15)$_3$phen	6.27	958[a]	1044	394	650	37.8
Tb(HFAASi-SBA-15)$_3$phen	...	460[b]	2174	...	...	...

[a]For the $^5D_0 \rightarrow {}^7F_2$ transition of Eu^{3+}.
[b]For the $^5D_4 \rightarrow {}^7F_5$ transition of Tb^{3+}.

Further, we selectively determined the emission quantum efficiencies of the $^5D_0$ excited state of the europium ion on the basis of the emission spectra and lifetimes of the $^5D_0$ emitting level. The detailed luminescent data are shown in Table II. Assuming that only nonradiative and radiative processes are essentially involved in the depopulation of the $^5D_0$ state, η can be defined as follows[33–37]:

$$\eta = A_r/(A_r + A_{nr}) \quad , \qquad (1)$$

Here, A_r and A_{nr} are radiative and nonradiative transition rates, respectively. A_r can also be obtained by summing over the radiative rates A_{0J} for each of the $^5D_0 \rightarrow {}^7F_J$ (J = 0–4) transitions. The branching ratio for the $^5D_0 \rightarrow {}^7F_{5,6}$ transitions can be neglected as they are not detected experimentally, whose influence can be ignored in the depopulation of the $^5D_0$ excited state. Since $^5D_0 \rightarrow {}^7F_1$ belongs to the isolated magnetic dipole transition, it is practically independent of the chemical environments around Eu^{3+}, and can be considered as an internal reference for the whole spectra, the experimental coefficients of spontaneous emission A_{0J} can be calculated according to the equation as follows:

$$A_{0J} = A_{01}(I_{0J}/I_{01})(\nu_{01}/\nu_{0J}) \quad , \qquad (2)$$

Here, A_{0J} is the experimental coefficients of spontaneous emission. A_{01} is the Einstein's coefficient of spontaneous emission between the $^5D_0$ and $^7F_1$ energy levels. In vacuum, A_{01} could be used as a value of 14.65 s^{-1}, whereas in the air atmosphere, the value of A_{01} can be determined to be 50 s^{-1} approximately ($A_{01} = n^3 A_{01(vac)}$),[19] when an average index of refraction n equal to 1.506 was considered. I_{01} and I_{0J} are the integrated intensities of the $^5D_0 \rightarrow {}^7F_1$ and $^5D_0 \rightarrow {}^7F_J$ transitions (J = 0–4) with ν_{01} and ν_{0J} ($\nu_{0J} = 1/\lambda_J$) energy centers, respectively. ν_{0J} refers to the energy barrier and can be determined with the emission peaks of $^5D_0 \rightarrow {}^7F_J$ emission transitions of Eu^{3+}. The emission intensity, I, is taken as the integrated intensity of the $^5D_0 \rightarrow {}^7F_{0-4}$ emission curves.

On the basis of the above discussion, the quantum efficiencies of mesoporous hybrid material Eu(HFAASi-SBA-15)$_3$phen can be determined as shown in Table II. In addition, compared with the hybrid Eu(HFAASi)$_3$phen (34.8%) reported in the literature,[19] the quantum efficiency of corresponding mesoporous hybrid material Eu(HFAASi-SBA-15)$_3$phen (37.8%) is higher, which shows that SBA-15 is an excellent host for the lanthanide β-diketone complex.

IV. CONCLUSIONS

In summary, the organic–inorganic mesoporous luminescent hybrid materials Ln(HFAASi-SBA-15)$_3$phen were obtained by linking the ternary lanthanide (Eu^{3+}, Tb^{3+}) complexes to the ordered SBA-15 mesoporous material by the modification of HFAA with TESPIC using a co-condensation method. The resulting materials Ln(HFAASi-SBA-15)$_3$phen all have high surface area and preserve mesoscopically ordered structures. Further investigation into the luminescent properties of Ln(HFAASi-SBA-15)$_3$phen mesoporous materials exhibits that the characteristic luminescence of the corresponding lanthanide ions (Ln^{3+}) through the intramolecular energy transfers from the modified ligand (HFAASi) to the lanthanide ions. The excellent luminescent properties of these materials, together with the uniform tunable pore sizes and the ordered hexagonal channel structure of the organic group functionalized SBA-15 mesoporous hybrid materials

https://doi.org/10.1557/jmr.2014.33 Published online by Cambridge University Press

will expand their applications in both optical and electronic areas.

ACKNOWLEDGMENTS

This work was supported by the Scientific Research Foundation of Hebei Province Education Department (No. Z2013015), the Doctoral Science Foundation of Hebei University of Science and Technology (No. QD201255), and the Xiaoli Foundation of Hebei University of Science and Technology (XL201257 and XL201250).

REFERENCES

1. C. Koeppen, S. Yamada, G. Jiang, A.F. Garito, and L.R. Dalton: Rare-earth organic complexes for polymer optical fiber and waveguide amplifiers. *J. Opt. Soc. Am. B: Opt. Phys.* **14**, 155 (1997).
2. J.M. Lehn: Perspectives in supramolecular chemistry-from molecular recognition towards molecular information processing and self-organization. *Angew. Chem. Int. Ed. Engl.* **29**, 1304 (1990).
3. M.D. McGehee, T.B. Bergstedt, C. Zhang, A.P. Saab, M.B. O'Regan, G.C. Bazan, V.I. Srdanov, and A.J. Heeger: Narrow bandwidth luminescence from blends with energy transfer from semiconducting conjugated polymers to europium complexes. *Adv. Mater.* **11**, 1349 (1999).
4. J. Kido and Y. Okamoto: Organo lanthanide metal complexes for electroluminescent materials. *Chem. Rev.* **102**, 2357 (2002).
5. H.R. Li, J. Lin, H.J. Zhang, L.S. Fu, Q.G. Meng, and S.B. Wang: Preparation and luminescence properties of hybrid materials containing europium(III) complexes covalently bonded to a silica matrix. *Chem. Mater.* **14**, 3651 (2002).
6. L.D. Carlos, R.A. Sá Ferreira, R.N. Pereira, M. Assuncao, and V.D.Z. Bermudez: White-light emission of amine-functionalized organic/inorganic hybrids: Emitting centers and recombination mechanisms. *J. Phys. Chem. B* **108**, 14924 (2004).
7. D.J. Zhang, X.M. Wang, Z.A. Qiao, D.H. Tang, Y.L. Liu, and Q.S. Huo: White-light emission of amine-functionalized organic/inorganic hybrids: Emitting centers and recombination mechanisms. *J. Phys. Chem. C* **114**, 12505 (2010).
8. X.M. Guo, H.D. Guo, L.S. Fu, R.P. Deng, W. Chen, J. Feng, S. Dang, and H.J. Zhang: Synthesis, spectroscopic properties, and stabilities of ternary europium complex in SBA-15 and periodic mesoporous organosilica: A comparative study. *J. Phys. Chem. C* **113**, 2603 (2009).
9. D.Y. Zhao, J.Y. Sun, Q.Z. Li, and G.D. Stucky: Morphological control of highly ordered mesoporous silica SBA-15. *Chem. Mater.* **12**, 275 (2000).
10. S. Madhugiri, A. Dalton, J. Gutierrez, J.P. Ferraris, and K.J. Balkus: Electrospun MEH-PPV/SBA-15 composite nanofibers using a dual syringe method. *J. Am. Chem. Soc.* **125**, 14531 (2003).
11. C.Y. Peng, H.J. Zhang, J.B. Yu, Q.G. Meng, L.S. Fu, H.R. Li, L.N. Sun, and X.M. Guo: Synthesis, characterization, and luminescence properties of the ternary europium complex covalently bonded to mesoporous SBA-15. *J. Phys. Chem. B* **109**, 15278 (2005).
12. L.S. Li, Y. Zhang, J.B. Yu, C.Y. Peng, and H.J. Zhang: Ternary lanthanide (Er^{3+}, Nd^{3+}, Yb^{3+}, Sm^{3+}, Pr^{3+}) complex-functionalized mesoporous SBA-15 materials that emit in the near-infrared range. *J. Photochem. Photobiol., A* **199**, 57 (2008).
13. C.Y. Peng, H.J. Zhang, Q.G. Meng, H.R. Li, J.B. Yu, J.F. Guo, and L.N. Sun: Synthesis and luminescence properties of SBA-15 functionalized with covalently bonded ternary europium complex. *Inorg. Chem. Commun.* **8**, 440 (2005).
14. Y. Li, B. Yan, and H. Yang: Construction, characterization, and photoluminescence of mesoporous hybrids containing europium(III) complexes covalently bonded to SBA-15 directly functionalized by modified beta-diketone. *J. Phys. Chem. C* **112**, 3959 (2008).
15. B. Yan and Y. Li: Luminescent ternary inorganic-organic mesoporous hybrids Eu(TTASi-SBA -15)phen: Covalent linkage in TTA directly functionalized SBA-15. *Dalton Trans.* **39**, 1480 (2010).
16. Y.J. Li and B. Yan: Lanthanide (Eu^{3+}, Tb^{3+})/β-diketone modified mesoporous SBA-15/organic polymer hybrids: Chemically bonded construction, physical characterization, and photophysical properties. *Inorg. Chem.* **48**, 8276 (2009).
17. Y.J. Li, L. Wang, and B. Yan: Photoactive lanthanide hybrids covalently bonded to functionalized periodic mesoporous organosilica (PMO) by calix[4]arene derivative. *J. Mater. Chem.* **21**, 1130 (2011).
18. Y.J. Li, B. Yan, and Y. Li: Lanthanide (Eu^{3+}, Tb^{3+}) centered mesoporous hybrids with 1,3-diphenyl-1,3-propanepione covalently linking SBA-15 (SBA-16) and poly(methylacrylic acid). *Chem. Asian J.* **5**, 1642 (2010).
19. C. Wang and B. Yan: Rare earth (Eu^{3+}, Tb^{3+}) centered composite gels Si-O-M (M = B, Ti) through hexafluoroacetyl-acetone building block: Sol-gel preparation, characterization and photoluminescence. *Mater. Res. Bull.* **46**, 2515 (2011).
20. M. Yu, J. Lin, and J. Fang: Silica spheres coated with YVO4: Eu^{3+} layers via sol–gel process: A simple method to obtain spherical core–shell phosphors. *Chem. Mater.* **17**, 1783 (2005).
21. M. Yu, J. Lin, Z. Wang, J. Fu, S. Wang, H.J. Zhang, and Y.C. Han: Fabrication, patterning, and optical properties of nanocrystalline YVO4: A (A = Eu^{3+}, Dy^{3+}, Sm^{3+}, Er^{3+}) phosphor films via sol–gel soft lithography. *Chem. Mater.* **14**, 2224 (2002).
22. Y.J. Li, B. Yan, and Y. Li: Luminescent lanthanide (Eu^{3+}, Tb^{3+}) ternary mesoporous hybrids with functionalized β-diketones (TTA, DBM) covalently linking SBA-15 and 2,2′-bipyridine (bpy). *Microporous Mesoporous Mater.* **131**, 82 (2010).
23. B. Yan, J.W. Wang, and Y.J. Li: Metallic inorganic/organic hybrid system through functionalized Schiff-base linkage: Molecular assembly, characterization and luminescence. *J. Alloys Compd.* **509**, 9240 (2011).
24. M. Kruk and M. Jaroniec: Gas adsorption characterization of ordered organic-inorganic nanocomposite materials. *Chem. Mater.* **13**, 3169 (2001).
25. W.H. Zhang, X.B. Lu, J.H. Xiu, Z.L. Hua, L.X. Zhang, M. Robertson, J.L. Shi, D.S. Yan, and J.D. Holmes: Synthesis and characterization of bifunctionalized ordered mesoporous materials. *Adv. Funct. Mater.* **14**, 544 (2004).
26. L.L. Kong, B. Yan, and Y. Li: Hybrid materials of SBA-15 functionalized by Tb^{3+} complexes of modified acetylacetone: Covalently bonded assembly and photoluminescence. *J. Alloys Compd.* **481**, 549 (2009).
27. W.Q. Fan, J. Feng, S.Y. Song, Y.Q. Lei, G.L. Zheng, and H.J. Zhang: Synthesis and optical properties of europium-complex-doped inorganic/organic hybrid materials built from oxo–hydroxo organotin nano building blocks. *Chem. Eur. J.* **16**, 1903 (2010).
28. J.P. Miranda, J. Zukerman-Schpector, P.C. Isolani, G. Vicentini, and L.B. Zinner: Synthesis and structure of lanthanide picrates with trans-1,3-dithiane-1,3-dioxide. *J. Alloys Compd.* **344**, 141 (2002).

https://doi.org/10.1557/jmr.2014.33 Published online by Cambridge University Press

29. E. Guillet, D. Imbert, R. Scopelliti, and J.C.G. Bünzli: Tuning the emission color of europium-containing ionic liquid-crystalline phases. *Chem. Mater.* **16**, 4063 (2004).
30. Y.J. Li, B. Yan, and L. Wang: Calix[4]arene derivative functionalized lanthanide (Eu, Tb) SBA-15 mesoporous hybrids with covalent bond: Assembly, characterization and photoluminescence. *Dalton Trans.* **40**, 6722 (2011).
31. K. Binnemans, P. Lenaerts, K. Driesen, and C. Gorller-Walrand: A luminescent tris(2-thenoyltrifluoroacetonato) europium(III) complex covalently linked to a 1,10-phenanthroline-functionalised sol-gel glass. *J. Mater. Chem.* **14**, 191 (2004).
32. O.L. Malta, H.F. Brito, J.F.S. Menezes, F.R.G.E. Silva, S. Alves, F.S. Farias, and A.V.M. DeAndrade: Spectroscopic properties of a new light- converting device Eu(thenoyltrifluoroacetonate)$_3$ 2(dibenzyl Sulfoxide). A theoretical analysis based on structural data obtained from a sparkle model. *J. Lumin.* **75**, 255 (1997).
33. O.L. Malta, M.A.C. DosSantos, L.C. Thompson, and N.K. Ito: Intensity parameters of 4f-4f transitions in the Eu(dipivaloylmethanate)$_3$ 1,10-phenanthroline complex. *J. Lumin.* **69**, 77 (1996).
34. E.E.S. Teotonio, J.G.P. Espynola, H.F. Brito, O.L. Malta, S.F. Oliveria, D.L.A. de Foria, and C.M.S. Izumi: Influence of the N-[methylpyridyl]acetamide ligands on the photoluminescent properties of Eu(iii)-perchlorate complexes. *Polyhedron* **21**, 1837 (2002).
35. M.H.V. Werts, R.T.F. Jukes, and J.W. Verhoeven: The emission spectrum and the radiative lifetime of Eu^{3+} in luminescent lanthanide complexes. *Phys. Chem. Chem. Phys.* **4**, 1542 (2002).
36. L.D. Carlos, V.D. Bermudez, R.A.S. Ferreira, L. Marques, and M. Assuncao: Sol–gel derived urea cross-linked organically modified silicates. 2. Blue-light emission. *Chem. Mater.* **11**, 581 (1999).
37. P.P. Lima, S.S. Nobre, R.O. Freire, S.A. Junior, L. Mafra, R.A.S. Ferreira, U. Pischel, O.L. Malta, and L.D. Carlos: Energy transfer mechanisms in organic-inorganic hybrids incorporating europium(III): A quantitative assessment by light emission spectroscopy. *J. Phys. Chem. C* **111**, 17627 (2007).

https://doi.org/10.1557/jmr.2014.33 Published online by Cambridge University Press